JGR Planets

RESEARCH ARTICLE
10.1029/2020JE006568

A Recharge Oscillator Model for Interannual Variability in Venus' Clouds

Pushkar Kopparla[1,2], Ashwin Seshadri[3], Takeshi Imamura[1], and Yeon Joo Lee[4]

[1]Graduate School of Frontier Sciences, The University of Tokyo, Kashiwa, Japan, [2]Center for Space and Habitability, University of Bern, Bern, Switzerland, [3]Centre for Atmospheric and Oceanic Sciences and Divecha Centre for Climate Change, Indian Institute of Science, Bengaluru, India, [4]Zentrum für Astronomie und Astrophysik, Technische Universität Berlin, Berlin, Germany

Key Points:

- A simple model is developed to explore relationships between convective activity in the cloud layer and cloud-base water abundance
- Sustained recharge-discharge oscillations exist within this model on interannual to decadal timescales
- The interannual to decadal sulfur dioxide variability at the cloud tops could be a result of these oscillations, instead of explosive volcanic injections

Supporting Information:

- Supporting Information 1

Correspondence to:
P. Kopparla,
pushkarkopparla@gmail.com

Citation:
Kopparla, P., Seshadri, A., Imamura, T., & Lee, Y. J. (2020). A recharge oscillator model for interannual variability in Venus' clouds. *Journal of Geophysical Research: Planets. 125*, e2020JE006568. https://doi.org/10.1029/2020JE006568

Received 11 JUN 2020
Accepted 9 OCT 2020

Abstract Sulfur dioxide is a radiatively and chemically important trace gas in the atmosphere of Venus and its abundance at the cloud tops has been observed to vary on interannual to decadal timescales. This variability is thought to come from changes in the strength of convection which transports sulfur dioxide to the cloud tops, although the dynamics behind such convective variability are unknown. Here, we propose a new conceptual model for convective variability that links the radiative effects of water abundance at the cloud-base to convective strength within the clouds, which in turn affects water transport within the cloud. The model consists of two coupled equations which are identified as a recharge-discharge oscillator. The solutions of the coupled equations are finite amplitude sustained oscillations in convective strength and cloud-base water abundance on 3–9 years timescales. The characteristic oscillation timescale is given by the geometric mean of the radiative cooling time and the eddy mixing time near the base of the convective clouds.

Plain Language Summary Water and sulfur dioxide are important trace gases in the atmosphere of Venus. The photolysis of sulfur dioxide in the upper clouds produces sulfuric acid, which forms the thick cloud decks characteristic of the planet's atmosphere. Sulfur dioxide abundances at the cloud top of Venus (about 70 km altitude) have been observed to oscillate on interannual to decadal timescales. In this paper, we use a simplified model of atmospheric dynamics and chemistry to outline the mechanism that causes such oscillations. The water abundance at the base of the clouds (about 47 km altitude), has a strong influence on the cloud-base heating and cloud level convection. The cloud level convective mixing in turn determines the gradient of water abundance in the cloud layer, and thereby the cloud-base water abundance. Thus, the convection and water abundance form a coupled system that oscillates on interannual to decadal timescales, which can explain the timescale of variability in the transport of sulfur dioxide to the cloud tops.

1. Introduction

The clouds of Venus are among the primary controls of the atmospheric radiative balance, and are composed of sulfuric acid, water and other sulfur-based aerosols which form from the photolysis of sulfur dioxide (Esposito et al., 1983). The main cloud deck can be resolved into three distinct regions, and ranges from 70 to 47 km in the atmosphere (Knollenberg & Hunten, 1980). The upper clouds are formed by the photochemical production of sulfuric acid from sulfur dioxide, the middle clouds by the droplet growth in the convective region, and lower clouds by condensation of sulfuric acid from the lower atmosphere on to the middle cloud droplet flux (Imamura & Hashimoto, 2001; Krasnopolsky & Pollack, 1994; Mills et al., 2007). Climate modeling studies of Venus have noted that the climate state is very sensitive to perturbations of SO_2, H_2O and cloud albedo (Bullock & Grinspoon, 2001; Hashimoto & Abe, 2001). Several decades of ground and space based observations of sulfur dioxide show that this trace gas is highly variable at the cloud tops at timescales of hours to decades (Encrenaz et al., 2016, 2020; Marcq et al., 2020; Vandaele et al., 2017a, 2017b, and references therein), varying by up to two orders of magnitude. Understanding the nature of this variability is critical to understanding the trajectory of Venus climate.

The deep atmosphere of Venus (~40 km) has sulfur dioxide and water abundances with mean values and variabilities of approximately 130 ± 50 and 30 ± 10 ppm (parts per million) (Barstow et al., 2012; Marcq et

al., 2008, 2018). These gases are then raised up to cloud tops at low latitudes by convective uplifting, where their concentrations decrease due to photodissociation to form sulfuric acid and other sulfur aerosols. At the cloud tops, sulfur dioxide abundance varies between 10 and 1,000 ppb (Vandaele et al., 2017b) and water 1–7 ppm (Encrenaz et al., 2016; Fedorova et al., 2008, 2016). The short-term (hourly daily) variability of sulfur dioxide is likely due to the localized variations of vertical mixing via small convective cells and its fast dissociation by photolysis (Marcq et al., 2013; Vandaele et al., 2017a). Indeed, such small scale convective variability is seen in recent radio observations of the cloud layer (Imamura et al., 2018). On decadal timescales, sulfur dioxide variability at the cloud top is characterized by strong intermittent injections from the troposphere followed by slow decays due to photolysis (Marcq et al., 2013; Vandaele et al., 2017a). While early studies attributed such injections to episodic volcanic activity (Esposito, 1984), more recent literature has shifted towards interpreting it in terms of variability of vertical mixing in the cloud layer (Krasnopolsky, 2012; Marcq et al., 2013). However, the dynamics driving such possibly periodic changes in the convective mixing have remained an open question till now (Marcq et al., 2018) and understanding variability on this interannual to decadal timescale is the focus of this paper. The observational record for these long period variations is about 40 years long, spanning observations from Pioneer Venus (Esposito, 1984) and Venus Express (Marcq et al., 2013, 2020) to the InfraRed Telescope Facility (NASA IRTF) (Encrenaz et al., 2020).

Outgoing thermal flux from the hot, deep atmosphere is largely absorbed near the cloud-base and is the driver of convective activity in the middle cloud layer (Lebonnois et al., 2015; Pollack et al., 1980). Recent radiative transfer studies found that trace gas abundances near the cloud-base, in particular water abundance, have a large effect on the heating of the cloud-base (Haus et al., 2015b; Lee et al., 2016) which should affect the strength of convective mixing. In this paper, we develop a framework to investigate how changes in water abundance near the cloud-base affect vertical mixing within the cloud, possibly giving rise to regular variations in water and sulfur-dioxide transport to cloud tops on decadal timescales. Section 2 describes the model setup and Section 3 examines the solutions to the model and discusses their implications as well as the limitations of the model. Section 4 summarizes the findings and suggests directions for future investigations.

2. Model Description

Our approach here will be to construct a simplified box-model to study variability within and below the cloud layer. In the following discussion, we describe the vertical regions of interest in the atmosphere as below (Titov et al., 2018):

1. Upper box is the photochemically dominated upper cloud region (57–70 km, green colored region in Figure 1)
2. Middle box is the convectively unstable middle cloud region (50–57 km, hatched region). We will refer to this region as the convective cloud or convective column
3. Lower box is the lower cloud where water abundance strongly influences thermal flux (47–50 km, blue colored region). We will refer to this region as the cloud-base

Note that by "convective cloud top" in this paper, we refer to the boundary between the middle and upper boxes in Figure 1, while "cloud top" will refer to the top of the upper box. The abovementioned vertical ranges are approximations, and the actual values of these altitudes change with time, latitude, and local time as seen from various studies (e.g., Barstow et al., 2012; Imamura et al., 2014; Tellmann et al., 2009).

2.1. Variability of Cloud Level Convection

Our first step is to describe the dependence of cloud level convection to changes in cloud-base thermal flux. As demonstrated by the radiative transfer modeling of Lee et al. (2016), the water abundance in the lower box has a significant effect on the net thermal flux at the cloud-base (also see Figure 1). The vertical gradient of the thermal flux is the radiative heating at that level. Since extrema occur near the boundaries of the cloud-base, we approximate the radiative heating flux at the cloud-base as the difference between the maximum and minimum values of the thermal flux in the lower box. Using this definition, we calculate the heating fluxes from the profiles shown in Figure 1 giving heating flux values of 47.29, 40.38, 36.08, and 33.07 Wm^{-2} as water abundance is varied from 20, 30, 40 to 50 ppm. This is approximately linear, and

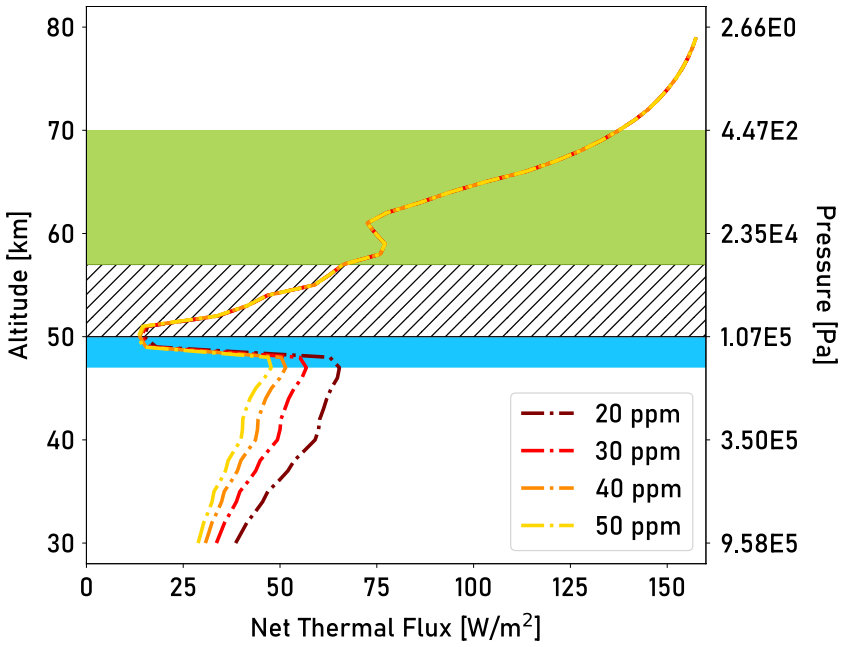

Figure 1. Simplified structure used in this work to represent the atmosphere of Venus. The green box shows the upper level dominated by photochemical clouds, the blue box shows the cloud-base and the hatched box in between shows the convective region. The thermal net flux profiles for different abundances of water in the blue box are from Lee et al. (2016), same as Figure 9c of that paper.

a least squares linear fit for these values yields a sensitivity of the heating flux to the water abundance of $-0.47\,\mathrm{Wm^{-2}ppm^{-1}}$. We parameterize this dependence of cloud-base heating on water abundance as a linear relationship:

$$Q_R\left(\left[H_2O\right]\right) - Q_R\left(\left[H_2O\right]^o\right) = -S_w\left(\left[H_2O\right] - \left[H_2O\right]^o\right) \quad (1)$$

where $Q_R([H_2O])$ is the cloud-base heating flux (in units of $\mathrm{Wm^{-2}}$) as a function of lower box water abundance, denoted by $[H_2O]$ in units of parts per million (ppm), $Q_R([H_2O]^o) = 47\ \mathrm{Wm^{-2}}$ is the cloud-base heating at an equilibrium water abundance of about $[H_2O]^o = 20$ ppm (Marcq et al., 2018) and $S_w = 0.47\ \mathrm{Wm^{-2}ppm^{-1}}$ is the sensitivity of the heating flux to the water abundance (A list of all variables used in the model is given in Table 1).

We relate changes in this thermal heating flux to changes in convective strength. The thermal heating changes the lapse rate and thus the static stability of the atmosphere, which is then adjusted to an adiabatic lapse rate by convective mixing wherever the lapse rate is superadiabatic. Typically, such a radiative-convective equilibrium is calculated recursively by adjusting the height of the convective layer once the radiative fluxes are known till the atmosphere is either statically stable or neutral at all altitudes and solar and thermal fluxes are balanced (e.g., Pierrehumbert, 2010, Chap 4 & 5). Here, we take a simpler approach to estimate the strength of convection with the changes in radiative forcing. At the cloud-base, a change in thermal heating from the equilibrium value of $Q_R([H_2O]^o)$ to a new value of $Q_R([H_2O])$ will result in the cloud-base temperature relaxing radiatively according to (Spiegel, 1957):

$$\frac{dT}{dt} = \frac{Q_R\left(\left[H_2O\right]\right) - Q_R\left(\left[H_2O\right]^o\right)}{\rho c_P L_b} \quad (2)$$

where $\rho \approx 2\mathrm{kgm^{-3}}$ is the atmospheric density at the cloud-base (Seiff et al., 1985), $c_P \approx 1{,}000\mathrm{JK^{-1}kg^{-1}}$ is the specific heat (Lebonnois et al., 2010) and $L_b = 3$ km is the height of the cloud-base. In the above equation,

Table 1
List of Variables Used

Symbol	Meaning
Q_R	IR heating at the cloud-base
$[H_2O]$	Water abundance at the cloud-base
$[H_2O]°$	Water abundance at the cloud-base at equilibrium
S_w	Sensitivity of IR heating to water abundance
T	Temperature of cloud-base
ΔT	Change in temperature of cloud-base
t	Time
ρ	Density of cloud-base
c_P	Specific heat at constant pressure of the atmosphere at cloud-base
L_b	Height of cloud-base
L	Height of convective cloud layer
$L°$	Height of convective cloud layer at equilibrium
ΔL	Change in height of convective cloud layer
Γ_{ad}	Dry adiabatic lapse rate
$[H_2SO_4]$	Sulfuric acid abundance at the cloud-base
$[H_2SO_4]°$	Sulfuric acid abundance at the cloud-base at equilibrium
$\Delta\left[H_2SO_4\right]$	Change in sulfuric acid abundance at the cloud-base
$\Delta\left[H_2O\right]$	Change in water abundance at the cloud-base
K	Eddy diffusivity in the convective cloud and cloud-base
$K°$	Eddy diffusivity in the convective cloud and cloud-base at equilibrium
H	Scale height of the atmosphere at the cloud base
$\left[H_2O\right]^{o}_{deep}$	Water abundance in the deep atmosphere (at 35 km)
t_{mix}	Chemical mixing timescale at cloud-base
v_{conv}	Vertical velocity in the convective cloud
α	Constant of proportionality between v_{conv} and L
L_{mix}	Eddy mixing length
x	Nondimensionalized water abundance anomaly at cloud-base
y	Nondimensionalized convective layer height anomaly
a,b	Coefficients in the nondimensionalized equations
T_{osc}	Time period of the oscillation

Note. Listed approximately in order of appearance in the text.

heat transport is assumed to be purely radiative, advective and eddy heat transport terms are neglected. This is an approximation, and can be justified on the basis that infrared radiation constitutes about 75%–85% of the upward heat transport even within the convective cloud (Imamura et al., 2014), and this fraction should be even higher at the cloud-base where there is no convection and eddy diffusivity is smaller than in the convective layer (Woo et al., 1982). Thus, the above equation will have errors of order 10%, but it is sufficiently accurate to understand the nature of temperature variability in response to flux changes.

We now explore the relationship between the convective strength in the clouds and the cloud-base temperature change. The cloud-base temperature changes only affect the temperature profile within the convective layer but are not expected to alter the thermal flux above the clouds due to the large infrared opacity of the

lower and middle cloud layer (Lee et al., 2016). Since a significant fraction of thermal flux from the top of the convective layer escapes directly to space through the relatively more transparent upper clouds (Lebonnois et al., 2015), we make the assumption that the temperature at the top of the convective cloud remains a constant irrespective of cloud-base temperature so that the net thermal flux above the clouds is invariant. So, if the cloud-base temperature changes by an amount ΔT, to keep the convective cloud top temperature constant, the convective cloud top height must change by an amount ΔL given by (Vallis et al., 2015):

$$\Delta L = \frac{\Delta T}{\Gamma_{ad}} \tag{3}$$

where $\Gamma_{ad} = 10^{o}\,\mathrm{Kkm}^{-1}$ is the adiabatic lapse rate in the convective clouds (Tellmann et al., 2009). We will use the convective layer height as a measure of convective strength and its variability. Combining Equations 2 and 3, we get a prognostic (i.e., an evolution) equation for the height of the convective cloud as a function of cloud-base heating:

$$\frac{dL}{dt} = \frac{\left(Q_R\left(\left[\mathrm{H_2O}\right]\right) - Q_R\left(\left[\mathrm{H_2O}\right]^{o}\right)\right)}{\rho c_P L_b \Gamma_{ad}} \tag{4}$$

2.2. Vertical Transport of Water

Chemical modeling of Venus has thus far focused primarily on calculating steady state abundances, since models which fully couple chemistry and dynamics still do not exist for Venus (Marcq et al., 2018; Shao et al., 2020). Thus, in this section we start with results from such steady state chemical calculations and then couple the shifts between steady states and dynamical variability. Within the clouds, the fluxes of water and sulfuric acid are coupled together and their vapor pressures are in liquid-vapor equilibrium with a sulfuric acid-water mixture at steady state (Krasnopolsky & Pollack, 1994). The downward eddy flux of sulfuric acid is equal to the production rate of sulfuric acid in the upper cloud and is given by the product of the eddy diffusivity and the vertical gradient of sulfuric acid abundance. Given a fixed rate of sulfuric acid production, the changes in the eddy diffusivity will alter the sulfuric acid gradient such that the downward eddy flux remains a constant (Krasnopolsky, 2015). Thus, cloud-base sulfuric acid abundances when chemical abundances have adjusted to changes in eddy diffusivity follow this relationship (Krasnopolsky, 2015):

$$\left[\mathrm{H_2SO_4}\right]K = \left[\mathrm{H_2SO_4}\right]^{o} K^{o} \tag{5}$$

where the right hand side values are at radiative equilibrium, and K is the vertical eddy diffusivity at the cloud-base. We assume that the eddy diffusivity remains invariant with height within the convective clouds and the cloud-base (Krasnopolsky, 2012). The implications of this assumption not being accurate are touched upon in Sections 3.1 and 3.4. Further, the assumption of a fixed sulfuric acid production rate implies that the upward fluxes of water and sulfur dioxide and the downward flux of sulfuric acid are also constant regardless of eddy diffusivity. This is a very strong assumption and it comes from using steady state chemical model results. Its caveats are further discussed in Section 3.4. Such a fixed flux condition usually implies that the gradients of the chemical abundance should follow an inverse proportionality relationship with the eddy diffusivity $\left(\mathrm{Flux} = K\frac{d\left[\mathrm{H_2SO_4}\right]}{dt} = \mathrm{constant}\right)$, but here the cloud-base abundances also follow this relationship, as expressed by Equation 5. This is because the cloud-base abundances are the lower boundary values set by the gradient within the clouds, so for example, a doubling of the gradient will double the cloud-base abundance.

The chemical abundance equilibrates to such changes in dynamics on a characteristic mixing timescale given by $t_{mix} = H^2/K^{o}$ (Krasnopolsky, 2012), where $H = 5$ km is the atmospheric scale height at the cloud-base. Then, the change in sulfuric acid concentration arising from a change in eddy diffusivity can be written using Equation 5 as:

$$\Delta\left[H_2SO_4\right] = \left[H_2SO_4\right] - \left[H_2SO_4\right]^o = \frac{\left[H_2SO_4\right]}{K^o}\left(K^o - K\right) \tag{6}$$

In the Krasnopolsky cloud models (Krasnopolsky, 2015; Krasnopolsky & Pollack, 1994) which calculate the abundances and fluxes of water and sulfuric acid within the clouds, the sum of water and sulfuric acid mixing ratios at the cloud-base (and below) are constrained to sum to a constant (equal to the deep atmospheric water mixing ratio) due a hydrogen element conservation constraint. The hydrogen element conservation is the condition that since water and sulfuric acid are the dominant hydrogen bearing species, and there is no significant loss of hydrogen e.g., to atmospheric escape or condensation), changes in the abundance of water and sulfuric acid must balance the upward and downward fluxes of hydrogen such that the total abundance of hydrogen at each vertical level remains a constant. Therefore, the change in the cloud-base water concentration has the same magnitude but opposite sign as that of the cloud-base sulfuric acid. These constraints give us two more relationships:

$$\Delta\left[H_2SO_4\right] = -\Delta\left[H_2O\right] \tag{7}$$

$$\left[H_2SO_4\right] + \left[H_2O\right] = \left[H_2O\right]^o_{deep} \tag{8}$$

where $\left[H_2O\right]^o_{deep}$ is the deep atmospheric water abundance where no sulfuric acid exists in the atmosphere, around 35 km altitude. Then, we can write Equation 6 in terms of water abundances using the above two relations as:

$$\Delta\left[H_2O\right] = -\left(\frac{\left[H_2O\right]^o_{deep} - \left[H_2O\right]}{K^o}\left(K^o - K\right)\right) \tag{9}$$

$$= \frac{\left[H_2O\right]^o_{deep} - \left[H_2O\right]}{K^o}\left(K - K^o\right) \tag{10}$$

Since the chemical compositions relax in response to dynamical perturbations over the mixing timescale t_{mix}, we can construct a simple prognostic equation for the evolution of water abundance:

$$\frac{d\left[H_2O\right]}{dt} = \frac{\Delta\left[H_2O\right]}{t_{mix}} \tag{11}$$

$$= \frac{\left[H_2O\right]^o_{deep} - \left[H_2O\right]}{K^o}\left(K - K^o\right) * \left(H^2 \,/\, K^o\right)^{-1} \tag{12}$$

$$= \frac{\left[H_2O\right]^o_{deep} - \left[H_2O\right]}{H^2}\left(K - K^o\right) \tag{13}$$

2.3. Closure Condition and Coupled Model Equations

We have found two prognostic equations and three unknowns—water abundance, convective layer height, and the eddy diffusivity. Thus, we need a closure condition linking the convective layer height and the eddy diffusivity to solve this system of equations. Turbulence-resolving numerical simulations of Venus' atmosphere found that the convective vertical velocity doubles for a doubling of the convective layer height

(Lefévre et al., 2018). This corresponds to a constant convective timescale, making the buoyant acceleration increase proportionally to height of the convective layer, and thus we can write a linear scaling relationship between convective velocity and convective layer height:

$$v_{conv} = \alpha L \tag{14}$$

Convective velocities are of order 1 ms^{-1} (Blamont et al., 1986) and convective layer height at equilibrium is $L^o = 7$ km (as defined in Section 2), so the constant of proportionality $\alpha = 1.4 \times 10^{-4} s^{-1}$. This value is the inverse of the convective timescale. The eddy diffusivity can then be written as:

$$K = v_{conv} * L_{mix} = \alpha L L_{mix} \tag{15}$$

where L_{mix} is a mixing length. Note that we have not made a distinction between thermal and momentum eddy diffusivities and the above value is derived from thermal considerations (layer height depends on cloud-base temperature, as defined in Section 2.1) but is used for estimating dynamical mixing of chemical species. Since the Prandtl number, which is the ratio of the momentum to the thermal diffusivity is of order unity and does not vary much with altitude from 45 to 60 km on Venus (Morellina et al., 2020), using a single value of eddy diffusivity for both is a crude but acceptable simplification. The relationship derived above indicates that higher thermal heating flux at the cloud base (represented by a larger convective layer height) leads to a higher eddy diffusivity, which is consistent with other numerical studies of eddy mixing in the Venus cloud layer (Yamamoto, 2014).

Estimating the appropriate magnitude for both K and L_{mix} is not straightforward. As summarized in the recent work of Bierson and Zhang (2019), dynamical studies such as cloud microphysics modeling (Imamura & Hashimoto, 2001; McGouldrick & Toon, 2007) support high values of K in the range of 10^2–10^3 $m^2 s^{-1}$, whereas chemical models (Krasnopolsky, 2012, 2015) prefer values of 1 $m^2 s^{-1}$ or lower to prevent large excess transport of trace gases such as sulfur dioxide to the upper atmosphere. Bierson and Zhang (2019) argue that this inconsistency indicates a gap in our understanding of the factors affecting chemical transport in the clouds, such as an unknown chemical sink or cloud interactions. Since our approach to modeling requires an eddy diffusivity consistent with chemistry and chemical mixing timescales, we employ $K_{zz} = 1$ $m^2 s^{-1}$ (Krasnopolsky, 2012), which gives an $L_{mix} = 1$ m. We acknowledge that this L_{mix} is much smaller than the ~1 km values calculated with the VEGA balloon observations (Blamont et al., 1986).

We can write the change in eddy diffusivity in terms of the change in layer height as:

$$\Delta K = K - K^o = \alpha L_{mix}\left(L - L^o\right) \tag{16}$$

Substituting Equation 1 into Equation 4 and Equation 16 into Equation 13, we end up with a coupled set of equations for water abundance and convective layer height:

$$\frac{d\left[H_2O\right]}{dt} = \frac{\alpha L_{mix}\left(L - L^o\right)\left(\left[H_2O\right]^o_{deep} - \left[H_2O\right]\right)}{H^2} \tag{17}$$

$$\frac{dL}{dt} = -\frac{S_w\left(\left[H_2O\right] - \left[H_2O\right]^o\right)}{\rho c_P L_b \Gamma_{ad}} \tag{18}$$

Given a pair of perturbed initial conditions for $[H_2O]$ and L, these equations can be integrated to give solutions for water abundance and convective strength as functions of time. These equations describe the effects of tendencies of both temperature and cloud-base water to relax to equilibrium values. Since these tendencies are coupled, the resulting behavior is an oscillation instead of first-order approach to equilibrium. We explore the nature of the solutions in the following section.

3. Results and Discussion

3.1. Solutions to the Coupled Equations

The model equations are structurally very similar to the set obtained by Yano and Plant (2012) [henceforth YP12] in their studies of convective cycles and represent a recharge-discharge oscillator. We note that while the equations have a similar structure, the present derivation represents very different physics on different timescales. However, in a mathematical sense they both involve similar coupled interactions, for example, the cloud base mass flux in YP12 and $[H_2O]$ in the present model are both being driven by departures in the cloud work function in YP12 and the depth of the convective layer here respectively. Furthermore, where in YP12 the cloud work function declines with an increase in the cloud base mass flux as buoyancy is released, the present model has the convective layer height decreasing with an increase in water abundance owing to reductions in the heating rate. As a result, we obtain similar dynamics, albeit on quite different timescales. We make the following substitution to nondimensionalize the present equations:

$$\left[\mathrm{H_2O}\right] = \left[\mathrm{H_2O}\right]^{\mathrm{o}}\left(1 + x\right) \tag{19}$$

$$L = L^{\mathrm{o}}\left(1 + y\right) \tag{20}$$

We take $\left[\mathrm{H_2O}\right]^{\mathrm{o}}_{\mathrm{deep}} = 1.5 * [\mathrm{H_2O}]^{\mathrm{o}} = 30$ ppm (Marcq et al., 2018) and $L^{\mathrm{o}} = 7$ km, as before. Variables x and y will be referred to as the nondimensional cloud-base water abundance anomaly and the convective layer height anomaly respectively. Thus, the Equations 17 and 18 become:

$$\frac{dx}{dt} = a\left(\frac{1}{2} - x\right)y \tag{21}$$

$$\frac{dy}{dt} = -bx \tag{22}$$

We can estimate the magnitudes of the coefficients a and b as follows:

$$a = \frac{\alpha L_{mix} L^{\mathrm{o}}}{H^2} = \frac{10^{-4} * 1 * 10^4}{10^7} \approx 10^{-7}\mathrm{s}^{-1} \approx \left(120\ \mathrm{days}\right)^{-1} \tag{23}$$

$$b = \frac{S_w\left[\mathrm{H_2O}\right]^{\mathrm{o}}}{\rho c_P L_b L^{\mathrm{o}} \Gamma_{ad}} = \frac{1 * 10}{1 * 10^3 * 10^3 * 10^4 * 10^{-2}} \approx 10^{-7}\mathrm{s}^{-1} \tag{24}$$

The coefficients have clear physical meanings: a is the inverse of the characteristic eddy mixing timescale in the convective clouds and b is the inverse of the radiative cooling timescale of the convective column, since it takes the form of the thermal flux over the heat capacity of the column. If the value of K is very different from the set value of 1 $\mathrm{m^2 s^{-1}}$, for example 0.1 $\mathrm{m^2 s^{-1}}$ and 100 $\mathrm{m^2 s^{-1}}$, the constant a will become approximately $(3\ \mathrm{years})^{-1}$ and $(1\ \mathrm{day})^{-1}$ respectively.

The steady-state of the model in Equations 21 and 22 is $x = y = 0$. The characteristic oscillation timescale for small perturbations to the steady of this coupled set of equations can be estimated from the linearized form of the Equations 21 and 22:

$$\frac{dx}{dt} = \frac{a}{2}y, \frac{dy}{dt} = -bx \tag{25}$$

The above two equations can be combined to yield the equation for a simple harmonic oscillator in either variable

$$\frac{d^2}{dt^2}\left(x, y\right) = -\frac{ab}{2}\left(x, y\right) \tag{26}$$

The time period of oscillation is given by

$$T_{osc} = 2\pi\sqrt{\frac{2}{ab}} \approx 3-9 \text{ years} \tag{27}$$

with the 3 years period for $[a] = 10^{-7}\text{s}^{-1}\left(K = 1\ \text{m}^2\text{s}^{-1}\right)$ and 9 years period for $[a] = 10^{-8}\text{s}^{-1}$ ($K = 0.1\ \text{m}^2\text{s}^{-1}$), $[b] = 10^{-7}\text{s}^{-1}$ is not changed. We vary a since our simplifying assumption of a height invariant eddy diffusivity is not always true. The eddy diffusivity near the cloud-base (45 km) was estimated from observations to be an order of magnitude smaller than near the top of the convective clouds (60 km) (Woo et al., 1982). Shorter mixing lengths, corresponding to smaller values of the eddy diffusivity, signify inefficient mixing and allow for the development and persistence of larger vertical concentration gradients and slower oscillations as a result.

Since the above is a rather large range for the oscillation period, a natural question to ask is: what is the appropriate timescale to consider when using this model to interpret observations of Venus? We note that the oscillation period is the geometric mean of the eddy mixing and radiative cooling timescales of the convective column multiplied by a constant value of 8.8. The radiative cooling timescale is fairly well understood since remote sensing and associated radiative modeling of Venus has a long heritage, but the mixing timescale near the cloud-base could very well vary by an order of magnitude in either direction and is not strongly constrained by continuous observations, since the last observationally constrained values of eddy diffusivity are from the 1980s (e.g., see Figure 3 of Bierson and Zhang (2019)). At this time, we cannot make a stronger prediction than to say the timescale is roughly interannual to decadal. Encrenaz et al. (2020) estimate that sulfur dioxide abundances at the cloud top decrease from a peak to a minimum value in about 5–7 years from 2008 to 2015, which is roughly consistent with the model timescale.

Furthermore, since Equation 26 does not have any damping or growing terms, oscillations resulting from an initial perturbation will maintain both their amplitude and period indefinitely. This is also true for the nonlinear set of equations (Equations 21 and 22). As we will see, its solutions persist indefinitely, giving rise to sustained oscillations around the steady state. The linearized system always has pure imaginary eigenvalues, since both a and b must be positive. Therefore, the qualitative behavior of the nonlinear system cannot be deduced from its linear approximation, because the conditions for equating their qualitative behaviors are not met. Eigenvalues of the linearized system are pure imaginary, and therefore not hyperbolic (nonzero real part) as required by the result of Hartman and Grobman giving conditions for the nonlinear phase portrait to qualitatively follow from the linearized one (Guckenheimer & Holmes, 2013).

Still it is possible to infer the behavior of the nonlinear system from explicit integration since, from Equations 21 and 22:

$$aydy = b\left\{1 - \frac{\frac{1}{2}}{\frac{1}{2}-x}\right\}dx \tag{28}$$

which is integrated for

$$ay^2 - b\left\{2x + \log\left(\frac{1}{2}-x\right)\right\} = C \tag{29}$$

where $C\left(x_0,y_0\right) = ay_0^2 - b\left\{2x_0 + \log\left(\frac{1}{2}-x_0\right)\right\}$ is constant in time, depending only on initial conditions $\left(x_0,y_0\right)$. Such "integrability" was demonstrated earlier for the recharge-discharge oscillator model of YP12. The present model's dynamics depends on function $f\left(x\right) = -b\left\{2x + \log\left(\frac{1}{2}-x\right)\right\}$ appearing in the above expression, which takes minimum value at $x = 0$ where its derivative $f'\left(x\right)$ vanishes. Everywhere, this function has positive second derivative $f''\left(x\right) = b\left(\frac{1}{2}-x\right)^{-2} > 0$, so it is convex. As a result $C(x,y)$ is convex

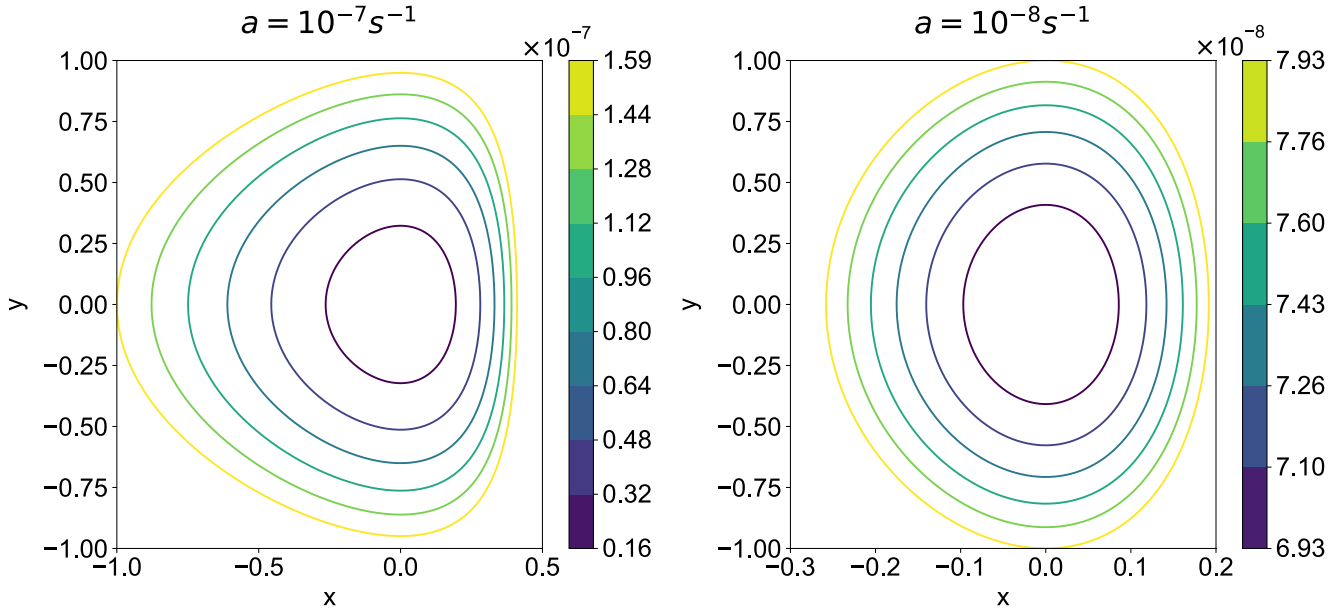

Figure 2. Phase plots showing the closed contours of the conserved quantity C for periodic solutions of the nonlinear model equations, where x and y are the nondimensional cloud-base water abundance anomaly and convective layer height anomaly respectively. The parameters are set to $[b] = 10^{-7}\mathrm{s}^{-1}$, while a is varied as shown in the panel title.

in both x and y, its contours are given by closed curves, and solutions of the nonlinear equations become periodic as show in Figure 2, with their time-evolution always conserving $C(x_0,y_0)$. Large-amplitude oscillations are quite asymmetric in the left panel, because unlike the symmetric quadratic potential for y, the logarithmic term makes $f(x)$ rise sharply as x approaches 1/2. We also note that the minimum values of x and y have a lower bound at −1. This is because the cloud-base water abundance and the lower height cannot be smaller than zero physically (Equations 21 and 22). Thus, the right panel remains close to the small-amplitude limit for x, since these values are already sufficient to cause large oscillations in y, of unit amplitude.

The period of oscillation of the nonlinear system is found by integrating Equation 21:

$$T_{osc} = \int_0^T dt = 2\int_{x_0}^{x_1} \frac{dx}{a\left(\frac{1}{2} - x\right)y} \tag{30}$$

where x_0 and x_1 are points of intersection between the particular trajectory and the x-axis, for which $y = 0$. Substituting for y from Equation 29 we obtain the period

$$T_{osc}\left(x_0\right) = 2\pi\sqrt{\frac{2}{ab}}g\left(x_0\right) \tag{31}$$

where the first part is identical to that of the linearized model in Equation 27 and the second factor absorbs the integral

$$g\left(x_0\right) = \int_{x_0}^{x_1(x_0)} \frac{dx}{\sqrt{2}\pi\left(\frac{1}{2} - x\right)\sqrt{2\left(x - x_0\right) + \log\frac{\frac{1}{2} - x}{\frac{1}{2} - x_0}}} \tag{32}$$

Figure 3 shows the factor $g(x_0)$ that increases the period for oscillations having large amplitude. In summary, the period of oscillation of the nonlinear system varies directly with the geometric mean of the eddy

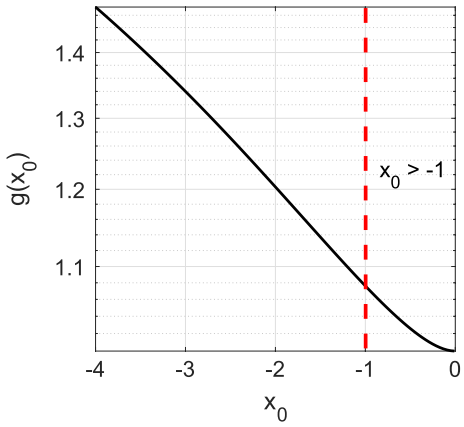

Figure 3. Function g showing the time period increase with respect to the simple harmonic period as a function of the minimum cloud-base water abundance anomaly, x_0. Physically speaking, the model is only valid to the right-side of the red line, such that the total cloud-base water abundance ($[H_2O]^o(1+x)$) always remains positive.

mixing timescale and the radiative cooling timescale, and grows weakly with the amplitude of the oscillation as measured by x_0. The model oscillations conserve the quantity $C(x,y)$ and small volume elements are recovered during the course of one period of the oscillation. The growth of volume elements is governed by the divergence of the vector field in Equations 21 and 22 and this, being equal to $-ay$, has a mean value of zero over a period of the oscillation. Therefore, this simple model cannot give rise to more complex dynamical behavior such as chaos, which requires a source of dissipation to compensate nonlinear growth.

Integrations of the model equations are shown in Figures 4 and 5 for small and large perturbations. The magnitude of changes in the linear regime are quite small and maybe difficult to observe. But the linear limit is nonetheless useful to derive the timescales of the oscillation and develop a physical intuition for how the coupled system of equations behaves in its simplest form. In the nonlinear limit the oscillations can be described as a recharge-discharge system: during the recharge phase the water abundance is nearly constant as the convective layer height decreases slowly. The discharge phase begins as the convective layer height approaches its minimum, during which time the cloud base water abundance begins to decrease rapidly. Water abundance reaches its minimum value and grows rapidly to reach its maximum value shortly after the convective layer height has reached its maximum.

3.2. Relationship to Observed Sulfur Dioxide Oscillations

Sulfur dioxide is transported to the cloud tops from the cloud-base by convective transport in the middle clouds upto about 57 km (though this height is variable as discussed earlier) and diffusive transport in the upper clouds upto 70 km. The sulfur dioxide abundances at the cloud tops having a strong relationship

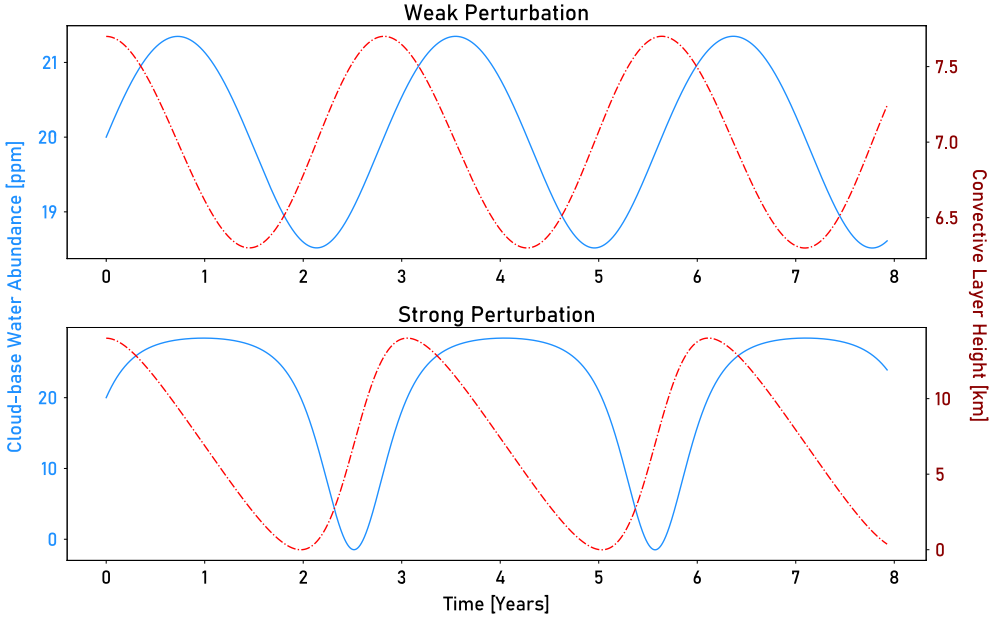

Figure 4. A simple first-order Eulerian scheme integration of the Equations 21 and 22 with $[a,b] = 10^{-7}s^{-1}$ showing interannual oscillations. The integrations were initialized with $[x,y] = [0,0.1]$ for the top panel and $[x,y] = [0,1]$ for the bottom panel. The blue solid line shows the cloud-base water abundance ($[H_2O]$), while the red dashed line shows the convective layer height (L). In the weak perturbation limit, the oscillations are harmonic and in the strong perturbation limit, they can be described as recharge-discharge oscillations.

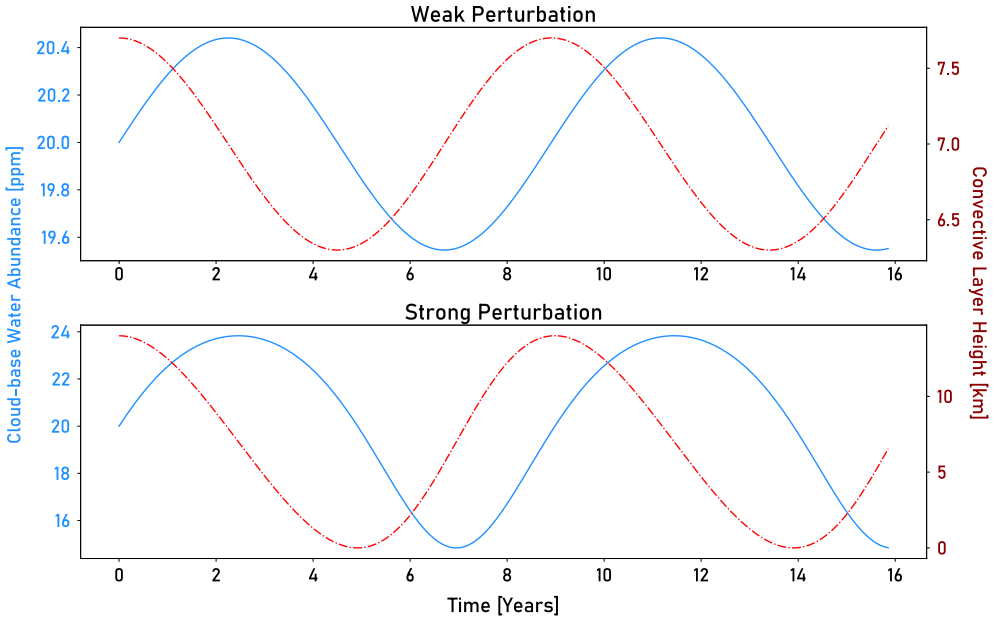

Figure 5. Same as Figure 4 but with $a = 10^{-8}\text{s}^{-1}$, showing decadal oscillations. As seen before in Figure 2, large changes in convective layer height produce only small changes in water abundance when the chemical mixing timescale is long. Thus, both the strong and weak perturbation limits behave similarly, like a harmonic oscillator.

to the convective mixing strength (as well as sulfur dioxide and water abundances at the cloud-base) has been established in multiple chemical modeling studies (Bierson & Zhang, 2019; Krasnopolsky, 2012, 2018; Parkinson et al., 2015). The dependence of cloud top sulfur dioxide on water abundance is complex, with correlated and anticorrelated behavior manifesting depending on whether water or sulfur dioxide is the relatively more abundant species at the convective cloud top (Shao et al., 2020).

Our model indicates that water abundance and convective strength vary out of phase by about a quarter cycle of the oscillation in the weak perturbation limit, it becomes necessary to consider fine vertical resolution to accurately model the upward transport under such changing conditions. Furthermore, we have used a very strong simplifying assumption in Section 2.2 that the sulfuric acid production rate remains a constant in the upper atmosphere, which implies that water and sulfur dioxide fluxes to the cloud top are a constant. Thus, variations in water and sulfur dioxide abundances at all altitudes in the cloud only occur in response to changes in eddy diffusivity to keep the net flux a constant. In reality, there is no reason that these fluxes should be a constant as convective strength varies, thus our model cannot be directly used to quantitatively predict changes in these fluxes.

In spite of these limitations, we can roughly discuss the changes in sulfur dioxide expected as a result of the oscillations described above. Krasnopolsky (2012) showed that as the convective layer top is moved by 10 km (from 55 to 65 km), the sulfur dioxide abundance at the cloud top varied by a factor of 30. For the strong perturbations shown in Figures 4 and 5, the change in layer height is about 14 km, which is slightly larger than that range. Thus, we would expect sulfur dioxide to vary between one and two orders of magnitude as a result of the convective layer height oscillations. This is in reasonable agreement with the observed magnitude of variability (Encrenaz et al., 2020; Marcq et al., 2013, 2020). Stronger quantitative arguments would require a more thorough modeling of atmospheric dynamics and chemistry and is a promising direction for future work.

Until now, the interannual variability of sulfur dioxide at the cloud tops was proposed to have two possible explanations: changes in vertical mixing due to atmospheric oscillations or volcanic injections of trace gases into the atmosphere (Encrenaz et al., 2020; Marcq et al., 2020). While the former explanation was preferred by some researchers due to Occam's razor (Krasnopolsky, 2012; Marcq et al., 2013), no mechanism was put forward to explain the existence of such an atmospheric oscillation. The model we described above provides just such a dynamical mechanism for interannual oscillations in the cloud layer mixing.

3.3. Model Predictions and Observables

The model predicts that the cloud-base water abundance and convective layer height should vary on interannual timescales. Furthermore, the model also predicts that the extrema in water abundance lag behind the extrema in convective layer height (see Figures 4 and 5). In the linear limit, the extrema in the two variables are separated by approximately 0.5 and 2 years for oscillations of period 3 and 9 years respectively. If this phase relationship does not hold, for example, if the water abundance peaks before the convective layer height peak, then the model introduced in this work can be falsified. In this section, we describe the nature of observations required to test these predictions.

The convective layer height can be observed using radio measurements, where the convective layer shows a distinctive adiabatic lapse rate as seen in observations from both Venus Express and Akatsuki (e.g., Imamura et al., 2017; Tellmann et al., 2009). A multiyear observational record of convective layer height would provide direct evidence of the oscillations proposed in this work. However, a direct analysis to extract possible interannual variations of the convective layer might be challenging, considering their limited spatial and temporal sampling coverages, which may be insufficient to distinguish latitudinal and local time dependences. Observations of water vapor abundance near the cloud-base would be the other way to check the predictions of the model described here. The 2.3 μm band is used to retrieve water vapor abundance in the 30–45 km subcloud altitude range on Venus. This region has been observed by several researchers with ground-based telescopes and space-based instruments such as VIRTIS on Venus Express (Arney et al., 2014; Marcq et al., 2008; Tsang et al., 2008). However, these studies have mostly focused on spatial variability and not on temporal variability. As shown in Figures 4 and 5, the cloud-base water abundance variability can have magnitudes of 10–20 ppm over a few years, which is much larger than observational uncertainties of order ±2–4 ppm (see Table 1 of Marcq et al. (2018) for a summary).

But the tricky issue about water vapor abundance retrieval at the 2.3 μm window is that there are no long-term baseline observations up to now. Even VIRTIS on Venus Express yielded only three years of data. Additionally, the weighting functions in the 2.3 μm band (which show the contribution function of thermal emission along altitudes to the observed signal) were rather broad, allowing limited vertical resolution of about 10 km (Haus et al., 2015a). Furthermore, the 2.3 μm band contains spectral contributions from clouds, carbon monoxide, water, OCS and sulfur dioxide (Marcq et al., 2008). In particular, all of the water abundance retrieval studies are affected by uncertainties in cloud aerosol properties, which are handled differently in each study (Arney et al., 2014; Marcq et al., 2008; Tsang et al., 2010). Thus, isolation of temporal trends across multiple studies is hard to achieve at this moment.

A long-term baseline analysis will be possible in the near future with the proposed ESA mission Envision. The radio science measurements would obtain convective layer height information, and the VenSpec suite of spectrographic instruments intends to observe water and sulfur dioxide above and below the clouds (Ghail et al., 2017). In addition to the data from the previous missions, these high-resolution measurements will have a sufficiently long time baseline capable of determining the existence and dominant periods of such oscillations. The ISRO Venus mission Shukrayaan-1 (Haider et al., 2018; ISRO, 2018), planned to launch in 2023, has spectrometers for studying atmospheric composition and a radio science instrument. Relevant data on water abundance and convective layer height may also come from this mission, but final instrument specifications are not publicly available at this time.

3.4. Model Limitations

In our model, we have idealized or simplified many complex processes. In this section, we explore the implications of our simplifying assumptions breaking down. First, the model is based upon perturbations from a stable equilibrium existing at a water abundance of $[H_2O]^o$ and convective layer height L^o. If, for example, the cloud-base water abundance is fixed to some nonequilibrium value by processes not included within our model, Equation 2 shows that the cloud-base temperature will either continuously rise or fall, tending to unphysical values over time. In reality, a new temperature equilibrium will be reached, but our simple model cannot search for such a new equilibrium as a more complex numerical model could. Thus, what we have treated as a closed system in our simplfied model is in reality an open system, and outside influences can force or damp these natural oscillations. Forcings can be caused by perturbations to water abundance by

supply of volatiles from continuous or sporadic volcanic outgassing (Esposito, 1984; Smrekar & Sotin, 2012) or changes in solar heating due to secular albedo changes over interannual timescales affecting convective layer height (Lee et al., 2019). Damping can be caused by heating and cooling influences on convection by changes in large scale circulation (Lefévre et al., 2018) or diffusive smoothing of water abundance anomalies by meridional circulation or vertical mixing in the deep atmosphere about which there is not much observational data (Sánchez-Lavega et al., 2017). The typical timescales for these processes are a few years, though the rate of volcanic outgassing is not well constrained and its effects on the atmosphere could be on much longer (centennial to millennial) timescales (Bullock & Grinspoon, 2001). If such forcings and dampenings are included, then the model will exhibit more complex dynamical behavior (possibly chaotic) instead of sustained finite amplitude oscillations.

Second, we made the simplifying assumption that chemical fluxes remain constant while eddy diffusivity changes in Section 2.2. This assumption comes from using the steady state chemical model results of Krasnopolsky, which enforce constant fluxes to maintain mass conservation within the model (Krasnopolsky, 1995). As noted earlier in Section 2.2, there are no fully coupled chemical dynamical models for Venus yet, therefore we are restricted to estimating how dynamical changes affect chemical profiles from such steady state models. In reality, there is no reason for chemical fluxes to remain constant within the dynamically changing atmosphere of Venus, and thus results based on such assumptions will underestimate the magnitude of variability in abundances.

Third, we have assumed that heating at the cloud-base depends on water abundance alone. While influences from other trace gases maybe small, cloud opacity is another significant source of cloud-base heating change (Lee et al., 2016) and cloud opacity is also known to vary on a timescale of about 150 days (McGouldrick & Toon, 2007), comparable to the 120 days timescale estimated for water abundance changes (Equation 23). The conditions for oscillations of the nature described here to exist in Venus' atmosphere are based on two tendencies:

1. A decrease in cloud-base infrared opacity will tend to decrease convective activity
2. Decrease in convective activity will tend to increase cloud-base infrared opacity

Would the changes in cloud mass or thickness yield these tendencies? If convective strength is weakened, the cloud mass supported by convection should decrease (Hashimoto & Abe, 2001). The reduction in cloud mass leads to cloud droplets falling from the convective middle clouds through the cloud-base (lower cloud) and vaporizing in the subcloud region. This represents a net transport of water and sulfuric acid from the middle and lower cloud to the subcloud region. Thus, a weakening in convection should result in thinner clouds (lower opacity) and higher subcloud water abundances (higher opacity), which has been observed (Tsang et al., 2010). Whether these changes result in a net higher or lower cloud-base heating is not easy to predict from first principles arguments and will require coupled microphysics and radiative transfer modeling. The possibility that cloud opacity plays an important role for interannual oscillations definitely exists and should be explored in future studies.

Finally, within our model we have not considered vertical or horizontal spatial variability, but rather have treated changes in water abundance or eddy diffusivity that are interpreted as global means. Nearly all quantities of interest, such as cloud height, water abundance, solar heating and convection show strong dependencies on latitude, longitude, altitude, and local time (Barstow et al., 2012; Encrenaz et al., 2019) as well as other transient regional scale changes (Arney et al., 2014; Tsang et al., 2010). Even eddy diffusivity, which we set to be uniform vertically, varies in magnitude depending on whether the region of interest is convective or stable (Imamura & Hashimoto, 2001), furthermore we have not considered the effects of mixing due to horizontal gradients. Thus, we expect that on Venus the interactions between all these different scales of variability will lead to a rich complexity in oscillations on many different spatial and temporal scales as opposed to the single timescale global oscillation we have derived with our simple model.

4. Conclusions

In this paper, we describe a hitherto unknown atmospheric dynamical mechanism that causes long period variability in the cloud layer of Venus. We explored relationships between cloud-base water abundance and convective strength. We find that that previously described dependences of infrared radiation on water

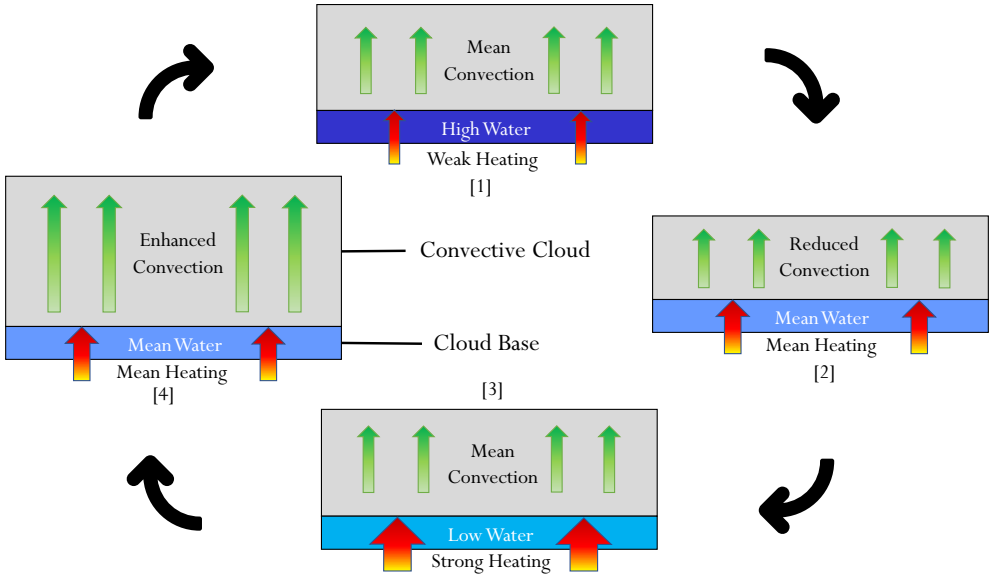

Figure 6. A schematic of the oscillations in the convective layer height and cloud-base water abundance described in this study. The oscillation is sustained because of the finite adjustment times of the cloud-base temperature (and thereby the convective layer height) and the water abundance to the cloud-base heating flux and convective mixing changes respectively.

abundance (Lee et al., 2016) and water abundance on eddy mixing (Krasnopolsky, 2012) can be coupled together. The two resulting prognostic equations represent a recharge-discharge oscillator. The atmospheric oscillation described here can explain the observed interannual sulfur dioxide variablity at the cloud tops without requiring episodic volcanic injections. It is a point of interest that a major interannual oscillation on Earth, the El Niño Southern Oscillation has also been described using a recharge oscillator paradigm (Jin, 1997). The model described in this work bears closer resemblance with the recharge-discharge oscillator describing departures from convective equilibrium (YP12).

A schematic of various stages of the oscillation are given in Figure 6. Physically speaking the oscillation can be described thus: A high water abundance anomaly at the base of the cloud leads to weakening of the cloud base forcing. The decline in forcing reduces the convective layer height and vertical mixing in the cloud layer. The decrease in vertical mixing reduces the water abundance at the cloud base leading to a low water anomaly, starting the other half of the oscillation. Alternately, the oscillation could also be initiated by a change in convective layer height which then changes the cloud-base water abundance and so forth. In the linear limit (caused by small perturbations to the equilibrium state), the oscillations are simple harmonic. In the nonlinear limit the oscillations can be described as a recharge-discharge system. The changes in convective layer height and cloud-base water abundance can strongly affect cloud top sulfur dioxide concentrations, which have been observed. However, our simplified model cannot quantify such variability, although that is a question of great interest for future studies with coupled chemical and dynamical modeling that builds on the mechanisms proposed in this work.

In the interest of obtaining simple, intuitive relationships, several complex processes were linearized. Thus, the model described here can only be fully justified in the weak perturbation limit where the water and convective strength anomalies are small compared to their equilibrium values. The nonlinear limit was also briefly touched upon and shows interesting behavior that maybe closer to the observations, particularly in that the convective strength appears to rise quickly and decrease gradually like the cloud top sulfur dioxide concentrations (Esposito, 1984; Marcq et al., 2013). There is also a weak tendency for the period to depend on the amplitude of the water abundance anomaly, with large anomalies causing oscillations of slightly longer periods. The linear dependence of convective layer height on cloud-base temperature (Equation 3) is a characteristic feature of many atmospheric shallow water systems (e.g., Heng, 2017, Chap 10), and may suggest that this system could be studied under a shallow water framework as a next step. A more thorough

treatment of the processes involved with a hierarchy of more sophisticated models would be very useful to better understand such long-period oscillations on Venus.

Data Availability Statement

Data and code for reproducing Figures 1–5 are openly available at Kopparla et al. (2020).

Acknowledgments
We would like to thank Javier Peralta, Yoshihisa Matsuda, and Kevin McGouldrick for comments and discussions which helped improve the paper. P. Kopparla was funded by the JSPS International Research Fellow program. Y. J. Lee has received funding from EU Horizon 2020 MSCA-IF No. 841432.

References

Arney G., Meadows V., Crisp D., Schmidt S. J., Bailey J., Robinson T. (2014). Spatially resolved measurements of H2O, HCl, CO, OCS, SO2, cloud opacity, and acid concentration in the Venus near-infrared spectral windows. *Journal of Geophysical Research: Planets*, *119*, (8), 1860–1891. http://dx.doi.org/10.1002/2014je004662.

Barstow J.K., Tsang C.C.C., Wilson C.F., Irwin P.G.J., Taylor F.W., McGouldrick K., et al. (2012). Models of the global cloud structure on Venus derived from Venus Express observations. *Icarus*, *217*, (2), 542–560. http://dx.doi.org/10.1016/j.icarus.2011.05.018.

Bierson C. J., Zhang X. (2020). Chemical Cycling in the Venusian Atmosphere: A Full Photochemical Model From the Surface to 110 km. *Journal of Geophysical Research: Planets*, *125*, (7), http://dx.doi.org/10.1029/2019je006159.

Blamont J. E., Young R. E., Seiff A., Ragent B., Sagdeev R., Linkin V. M., (1986). Implications of the VEGA Balloon Results for Venus Atmospheric Dynamics. *Science*, *231*, (4744), 1422–1425. http://dx.doi.org/10.1126/science.231.4744.1422.

Bullock M, & Grinspoon, D H (2001). The Recent Evolution of Climate on Venus. *Icarus*, *150*, (1), 19–37. http://dx.doi.org/10.1006/icar.2000.6570.

Encrenaz T., Greathouse T. K., Marcq E., Sagawa H., Widemann T., Bézard B., et al. (2019). HDO and SO2 thermal mapping on Venus. *Astronomy & Astrophysics*, *623*, A70http://dx.doi.org/10.1051/0004-6361/201833511.

Encrenaz T., Greathouse T. K., Marcq E., Sagawa H., Widemann T., Bézard B., et al. (2020). HDO and SO2 thermal mapping on Venus. *Astronomy & Astrophysics*, *639*, A69http://dx.doi.org/10.1051/0004-6361/202037741.

Encrenaz T., Greathouse T. K., Richter M. J., DeWitt C., Widemann T., Bézard B., et al. (2016). HDO and SO₂ thermal mapping on Venus. *Astronomy & Astrophysics*, *595*, A74http://dx.doi.org/10.1051/0004-6361/201628999.

ESPOSITO L. W. (1984). Sulfur Dioxide: Episodic Injection Shows Evidence for Active Venus Volcanism. *Science*, *223*, (4640), 1072–1074. http://dx.doi.org/10.1126/science.223.4640.1072.

Esposito, L., Knollenberg, R., Marov, M., Toon, O., & Turco, R. (1983). The clouds and hazes of venus. D. M. Hunten L. Colin T. M. Donahue & V. I. Moroz *Venus* , 484–564). Tucson, AZ: University of Arizona Press.

Fedorova, A., Korablev, O., Vandaele, A.-C., Bertaux, J.-L., Belyaev, D., Mahieux, A., et al. (2008). HDO and H_2O vertical distributions and isotopic ratio in the Venus mesosphere by solar occultation at infrared spectrometer on board venus express. *Journal of Geophysical Research: Planets*, *113*(E5), https://doi.org/10.1029/2008je003146.

Fedorova, A., Marcq, E., Luginin, M., Korablev, O., Bertaux, J.-L., & Montmessin, F. (2016). Variations of water vapor and cloud top altitude in the Venus mesosphere from spicav/vex observations. *Icarus*, *275*, 143–162. https://doi.org/10.1016/j.icarus.2016.04.010.

Ghail, R., Wilson, C., Widemann, T., Bruzzone, L., Dumoulin, C., Helbert, J., et al. (2017). Envision: Understanding why our most earth-like neighbour is so different. *arXiv preprint arXiv:1703.09010*.

Guckenheimer, J., & Holmes, P. (2013). Nonlinear oscillations, dynamical systems, and bifurcations of vector fields (Vol. 42). Springer Science & Business Media. https://doi.org/10.1007/978-1-4612-1140-2.

Haider, S. A., Bhardwaj, A., Shanmugam, M., Goyal, S., Sheel, V., Pabari, J., & Prasad Karanam, D. (2018). Indian Mars and Venus missions: Science and exploration. *Cosp*, *42*, B4–1.

Hashimoto, G. L., & Abe, Y. (2001). Predictions of a simple cloud model for water vapor cloud albedo feedback on Venus. *Journal of Geophysical Research*, *106*(E7), 14675–14690. https://doi.org/10.1029/2000JE001266.

Haus, R., Kappel, D., & Arnold, G. (2015a). Lower atmosphere minor gas abundances as retrieved from Venus express VIRTIS-M-IR data at 2.3 μm. *Planetary and Space Science*, *105*, 159–174. https://doi.org/10.1016/j.pss.2014.11.020.

Haus, R., Kappel, D., & Arnold, G. (2015b). Radiative heating and cooling in the middle and lower atmosphere of Venus and responses to atmospheric and spectroscopic parameter variations. *Planetary and Space Science*, *117*, 262–294. https://doi.org/10.1016/j.pss.2015.06.024.

Heng, K. (2017). *Exoplanetary atmospheres: Theoretical concepts and foundations*. Princeton University Press. https://doi.org/10.2307/j.ctvc77ddr.

Imamura, T., Ando, H., Tellmann, S., Pätzold, M., Häusler, B., & Yamazaki, A. (2017). Initial performance of the radio occultation experiment in the Venus orbiter mission Akatsuki. *Earth, Planets and Space*, *69*(1), 1–11. https://doi.org/10.1186/s40623-017-0722-3.

Imamura, T., & Hashimoto, G. L. (2001). Microphysics of Venusian clouds in rising tropical air. *Journal of the Atmospheric Sciences*, *58*(23), 3597–3612. https://doi.org/10.1175/1520-0469(2001)058<3597:MOVCIR>2.0.CO;2.

Imamura, T., Higuchi, T., Maejima, Y., Takagi, M., Sugimoto, N., Ikeda, K., & Ando, H. (2014). Inverse insolation dependence of Venus cloud-level convection. *Icarus*, *228*, 181–188. https://doi.org/10.1016/j.icarus.2013.10.012.

Imamura, T., Miyamoto, M., Ando, H., Häusler, B., Pätzold, M., Tellmann, S., et al. (2018). Fine vertical structures at the cloud heights of Venus revealed by radio holographic analysis of Venus express and Akatsuki radio occultation data. *Journal of Geophysical Research: Planets*, *123*(8), 2151–2161. https://doi.org/10.1029/2018JE005627.

ISRO. (2018). *Announcement of opportunity (ao) to international science community for space-based experiments to study* venus. https://www.isro.gov.in/sites/default/files/aovenus.pdf

Jin, F.-F. (1997). An equatorial ocean recharge paradigm for ENSO. Part I: Conceptual model. *Journal of the Atmospheric Sciences*, *54*(7), 811–829. https://doi.org/10.1175/1520-0469(1997)054<0811:AEORPF>2.0.CO;2.

Knollenberg, R., & Hunten, D. (1980). The microphysics of the clouds of Venus: Results of the pioneer Venus particle size spectrometer experiment. *Journal of Geophysical Research*, *85*(A13), 8039–8058. https://doi.org/10.1029/JA085iA13p08039.

Kopparla, P., Seshadri, A., Imamura, T., & Lee, Y. J. (2020). [Dataset] A Recharge Oscillator Model for Interannual Variability in Venus Clouds. https://doi.org/10.5281/zenodo.4003013

Krasnopolsky, V. A. (1995). Uniqueness of a solution of a steady state photochemical problem: Applications to Mars. *Journal of Geophysical Research*, *100*(E2), 3263–3276. https://doi.org/10.1029/94JE03283.

Krasnopolsky, V. A. (2012). A photochemical model for the Venus atmosphere at 47–112 km. *Icarus*, *218*(1), 230–246. https://doi.org/10.1016/j.icarus.2011.11.012.

Krasnopolsky, V. A. (2015). Vertical profiles of H_2O, H_2SO_4, and sulfuric acid concentration at 45–75 km on venus. *Icarus*, *252*, 327–333. https://doi.org/10.1016/j.icarus.2015.01.024.

Krasnopolsky, V. A. (2018). Disulfur dioxide and its near-UV absorption in the photochemical model of Venus atmosphere. *Icarus*, *299*, 294–299. https://doi.org/10.1016/j.icarus.2017.08.013.

Krasnopolsky, V. A., & Pollack, J. (1994). H_2O-H_2SO_4 system in Venus' clouds and OCS, CO, and H_2SO_4 profiles in Venus' troposphere. *Icarus*, *109*(1), 58–78. https://doi.org/10.1006/icar.1994.1077.

Lebonnois, S., Eymet, V., Lee, C., & Vatant d'Ollone, J. (2015). Analysis of the radiative budget of the Venusian atmosphere based on infrared net exchange rate formalism. *Journal of Geophysical Research: Planets*, *120*(6), 1186–1200. https://doi.org/10.1002/2015JE004794.

Lebonnois S., Hourdin F., Eymet V., Crespin A., Fournier R., Forget F. (2010). Superrotation of Venus' atmosphere analyzed with a full general circulation model. *Journal of Geophysical Research*, *115*, (E6), http://dx.doi.org/10.1029/2009je003458.

Lee, Y. J., Jessup, K.-L., Perez-Hoyos, S., Titov, D. V., Lebonnois, S., Peralta, J., et al. (2019). Long-term variations of Venus's 365 nm albedo observed by Venus express, Akatsuki, MESSENGER, and the Hubble Space Telescope. *The Astronomical Journal*, *158*(3), 126. https://doi.org/10.3847/1538-3881/ab3120.

Lee, Y. J., Sagawa, H., Haus, R., Stefani, S., Imamura, T., Titov, D. V., & Piccioni, G. (2016). Sensitivity of net thermal flux to the abundance of trace gases in the lower atmosphere of Venus. *Journal of Geophysical Research: Planets*, *21*(9), 1737–1752. https://doi.org/10.1002/2016JE005087.

Lefévre, M., Lebonnois, S., & Spiga, A. (2018). Three-dimensional turbulence resolving modeling of the Venusian cloud layer and induced gravity waves: Inclusion of complete radiative transfer and wind shear. *Journal of Geophysical Research: Planets*, *123*(10), 2773–2789. https://doi.org/10.1029/2018JE005679.

Marcq, E., Bertaux, J.-L., Montmessin, F., & Belyaev, D. (2013). Variations of sulphur dioxide at the cloud top of Venus's dynamic atmosphere. *Nature Geo-Science*, *6*(1), 25. https://doi.org/10.1038/ngeo1650.

Marcq, E., Bézard, B., Drossart, P., Piccioni, G., Reess, J., & Henry, F. (2008). A latitudinal survey of CO, OCS, H_2O, and SO_2 in the lower atmosphere of Venus: Spectroscopic studies using VIRTIS-H. *Journal of Geophysical Research*, *113*(E5), .https://doi.org/10.1029/2008JE003074.

Marcq, E., Jessup, K. L., Baggio, L., Encrenaz, T., Lee, Y. J., Montmessin, F., et al. (2020). Climatology of SO_2 and UV absorber at Venus' cloud top from SPICAV-UV nadir dataset. *Icarus*, *335*, 113368. https://doi.org/10.1016/j.icarus.2019.07.002.

Marcq, E., Mills, F. P., Parkinson, C. D., & Vandaele, A. C. (2018). Composition and chemistry of the neutral atmosphere of Venus. *Space Science Reviews*, *214*(1), 10. https://doi.org/10.1007/s11214-017-0438-5.

McGouldrick, K., & Toon, O. B. (2007). An investigation of possible causes of the holes in the condensational Venus cloud using a microphysical cloud model with a radiative-dynamical feedback. *Icarus*, *191*(1), 1–24. https://doi.org/10.1016/j.icarus.2007.04.007.

Mills, F. P., Esposito, L. W., & Yung, Y. L. (2007). Atmospheric composition, chemistry, and clouds. *Geophysical Monograph Series*, In L. Esposito, E. R. Stofan, & T. E. Cravens (Eds.), Exploring Venus as a terrestrial planet, 176, (73–100). https://doi.org/10.1029/176GM06.

Morellina S., Bellan J., Cutts J. (2020). Global thermodynamic, transport-property and dynamic characteristics of the Venus lower atmosphere below the cloud layer. *Icarus*, *350*, 113761http://dx.doi.org/10.1016/j.icarus.2020.113761.

Parkinson, C. D., Gao, P., Esposito, L., Yung, Y., Bougher, S., & Hirtzig, M. (2015). Photochemical control of the distribution of Venusian water. *Planetary and Space Science*, *113*, 226–236. https://doi.org/10.1016/j.pss.2015.02.015.

Pierrehumbert, R. T. (2010). *Principles of planetary climate*. Cambridge University Press. https://doi.org/10.1017/CBO9780511780783.

Pollack, J. B., Toon, O. B., & Boese, R. (1980). Greenhouse models of Venus' high surface temperature, as constrained by pioneer Venus measurements. *Journal of Geophysical Research*, *85*(A13), 8223–8231. https://doi.org/10.1029/JA085iA13p08223.

Sánchez-Lavega, A., Lebonnois, S., Imamura, T., Read, P., & Luz, D. (2017). The atmospheric dynamics of Venus. *Space Science Reviews*, *212*(3–4), 1541–1616. https://doi.org/10.1007/s11214-017-0389-x.

Seiff, A., Schofield, J., Kliore, A., Taylor, F., Limaye, S., Revercomb, H., et al. (1985). Models of the structure of the atmosphere of Venus from the surface to 100 kilometers altitude. *Advances in Space Research*, *5*(11), 3–58. https://doi.org/10.1016/0273-1177(85)90197-8.

Shao W. D., Zhang X., Bierson C. J., Encrenaz T. (2020). Revisiting the Sulfur-Water Chemical System in the Middle Atmosphere of Venus. *Journal of Geophysical Research: Planets*, *125*, (8), https://doi.org/10.1029/2019je006195.

Smrekar, S. E., & Sotin, C. (2012). Constraints on mantle plumes on Venus: Implications for volatile history. *Icarus*, *217*(2), 510–523. https://doi.org/10.1016/j.icarus.2011.09.011.

Spiegel, E. A. (1957). The smoothing of temperature fluctuations by radiative transfer. *The Astrophysical Journal*, *126*, 202. https://doi.org/10.1086/146386.

Tellmann, S., Pätzold, M., Häusler, B., Bird, M. K., & Tyler, G. L. (2009). Structure of the Venus neutral atmosphere as observed by the radio science experiment VeRa on Venus Express. *Journal of Geophysical Research*, *114*(E9), .https://doi.org/10.1029/2008JE003204.

Titov, D. V., Ignatiev, N. I., McGouldrick, K., Wilquet, V., & Wilson, C. F. (2018). Clouds and hazes of Venus. *Space Science Reviews*, *214*(8), 126. https://doi.org/10.1007/s11214-018-0552-z.

Tsang, C. C., Irwin, P. G., Wilson, C. F., Taylor, F. W., Lee, C., de Kok, R., et al. (2008). Tropospheric carbon monoxide concentrations and variability on Venus from Venus Express/Virtis-M observations. *Journal of Geophysical Research*, *113*(E5), .https://doi.org/10.1029/2008JE003089.

Tsang, C. C., Wilson, C. F., Barstow, J. K., Irwin, P. G., Taylor, F. W., Mc-Gouldrick, K., et al. (2010). Correlations between cloud thickness and sub-cloud water abundance on Venus. *Geophysical Research Letters*, *37*(2).https://doi.org/10.1029/2009GL041770.

Vallis, G., Rosenblum, E., & Payne, A. (2015). Technical report: 2014 geophysical fluid dynamics summer study program: Climate physics and dynamics. *Lecture*, *4*, 36–38. https://doi.org/10.1575/1912/7569

Vandaele, A. C., Korablev, O., Belyaev, D., Chamberlain, S., Evdokimova, D., Encrenaz, T., et al. (2017a). Sulfur dioxide in the Venus atmosphere: II. Spatial and temporal variability. *Icarus*, *295*, 1–15. https://doi.org/10.1016/j.icarus.2017.05.001.

Vandaele, A. C., Korablev, O., Belyaev, D., Chamberlain, S., Evdokimova, D., Encrenaz, T., et al. (2017b). Sulfur dioxide in the Venus atmosphere: I. Vertical distribution and variability. *Icarus*, *295*, 16–33. https://doi.org/10.1016/j.icarus.2017.05.003.

Woo, R., Armstrong, J., & Kliore, A. (1982). Small-scale turbulence in the atmosphere of Venus. *Icarus*, *52*(2), 335–345. https://doi.org/10.1016/0019-1035(82)90116-6.

Yamamoto, M. (2014). Idealized numerical experiments on microscale eddies in the Venusian cloud layer. *Earth, Planets and Space*, *66*(1), 27. https://doi.org/10.1186/1880-5981-66-27.

Yano, J.-I., & Plant, R. (2012). Finite departure from convective quasi-equilibrium: Periodic cycle and discharge–recharge mechanism. *Quarterly Journal of the Royal Meteorological Society*, *138*(664), 626–637. https://doi.org/10.1002/qj.957.